

# A Fourier Method Solution for the Time Dependent Schrödinger Equation as a Tool in Molecular Dynamics

D. KOSLOFF

*Department of Geophysics, Tel-Aviv University, Tel-Aviv, Israel 69978*

AND

R. KOSLOFF\*

*Department of Physical Chemistry and  
The Fritz Haber Research Center for Molecular Dynamics,  
The Hebrew University, Jerusalem, Israel 91904*

Received June 15, 1982; revised November 30, 1982

A new method is presented for the solution of the time dependent Schrödinger equation in its application to physical and chemical molecular phenomena. The method is based on discretizing space and time on a grid, and using the Fourier method to produce both spatial derivatives, and second order differencing for time derivatives. The method conserves norm and energy, and preserves quantum mechanical commutation relations. One- and two-dimensional examples, where a comparison to analytic results is possible, are investigated.

## I. INTRODUCTION

Many phenomena of physics and chemistry have a common dynamical evolution pattern. This pattern begins with an initial state which under the influence of the potentials, evolves through time to produce a final asymptotic state. Among such phenomena are chemical reactions, photodissociation, unimolecular breakdown, surface scattering, and desorption. The present study presents a numerical solution based on quantum mechanics for the common pattern, or for the time dependent evolution of the state of the system. The importance of exact numerical solutions is twofold, first these solutions give a quantitative description of physical problems and also are of use as a bench mark to check approximation methods and to define their range of validity.

\* Bat-Sheva Fellow.

In quantum mechanics the state of the system is represented by the wave function  $\psi$ , and the time evolution is governed by the Schrödinger equation

$$i \frac{\partial \psi}{\partial t} = \hat{H} \psi, \quad (1.1)$$

where  $\hat{H}$  is the Hamiltonian operator of the system and the initial state is  $\psi_0$ . (In this work atomic units are used in which  $\hbar = 1$ , and the mass is given in units of the electron mass). Solution of the Schrödinger equation provides all dynamical information on the physical system. A good integrating scheme for the Schrödinger equation will have the following qualities: it has to provide an approximation to the wave function with any predetermined precision: it has to be stable to round-off errors in the computation: it has to be general enough to deal with any physical potential and initial wavepacket; and the numerical algorithm has to be fast enough to obtain solutions in finite computation time.

Reviewing previous work on numerical solutions for dynamical molecular systems, the conventional approach has been one of stationary solutions with appropriate boundary conditions [1–7]. Time dependent solutions have been obtained by expansion of the initial state in stationary solutions [8]. This stationary approach has become a mature field which has developed efficient algorithms for finding the stationary solutions, such as the variational methods for bound states, close coupling methods, and the  $R$  matrix methods for scattering states. However, the stationary approach has proven limited when dealing with time dependent physical systems, primarily because of the added complexity of expansion needed to produce the time dependent solution.

The direct time dependent approach in previous studies has provided clearer physical interpretation than the stationary approach but seldom has been used as a computational tool. It has the advantage of unifying the bound and scattering problems, such as in the work of Lee and Heller [9] which uses a time dependent variational method [10]. There has also been a use of the finite difference method [11, 12]. To date, however, none of the existing methods can comply with the criteria for good numerical approximation as mentioned above.

In this present paper, a Fourier or pseudo spectral solution for the time dependent Schrödinger equation is presented. The Fourier method has been actively applied in the last decade to solutions of partial differential equations [13–19] such as the acoustical equation, the KDV equation [14], the diffusion equation [15], and the Navier–Stokes equation. The basic idea behind the method is to use the properties of the discrete Fourier transform to approximate spatial derivatives. Time derivatives are approximated by differencing.

The main advantages which the method possesses are simplicity and a high order of accuracy. These features allow a relatively small grid size for representing the problem, an extremely important factor in multidimensional problems. An important qualitative advantage of the method is that it maps the true Hilbert space of the problem to a discrete one. This mapping conserves the Hermitian quality and the

commutation relations of the operators which are associated with the actual observables.

In the next section we present the Fourier method application to the Schrödinger equation and discuss its features. Next, one- and two-dimensional examples are presented which test the solution scheme for different types of potentials.

## II. DETAILS OF THE FOURIER METHOD FOR THE TIME DEPENDENT SCHRÖDINGER EQUATION

The central idea behind the numerical approximation is to discretize the Hilbert space of the problem, and to construct a new Hilbert space in which Hermitian operators are mapped into Hermitian operators. In the Fourier method [16], space and time are discretized with a uniform grid. Let  $\psi^n(i_1, i_2, i_3, \dots, i_N)$  denote the wave function in  $N$ -dimensional Cartesian space at location  $X_m = (i_m - 1)\Delta X_m$  and at time  $t = (n - 1)\Delta t$ , where  $\Delta X_m$  and  $\Delta t$  represent the increment in the  $m$ th spatial coordinate and in time, respectively. With this discretization, the time dependent Schrödinger equation becomes

$$i \frac{\partial \psi^n}{\partial t}(i_1, i_2, \dots, i_N) = \hat{H}^n \psi^n(i_1, i_2, \dots, i_N) \quad (2.1)$$

with  $\hat{H}^n = -(1/2m)\hat{\nabla}^2 + \hat{V}^n$ .  $\hat{V}^n$  is the time dependent potential and  $\nabla^2$  is the  $N$ -dimensional Laplacian operator.

The numerical solution of (2.1) includes both spatial derivatives as well as temporal derivatives. The spatial approximation for the derivative utilizes the property of the Fourier transforms that a derivative in the spatial domain becomes a multiplication by  $iK_{i_l}$  in the spatial frequency domain, where  $K_{i_l}$  is the wave number corresponding to the  $l$ -spatial coordinate. The Laplacian operator in (2.1) is thus obtained by performing an  $N$ -dimensional Fourier transform on  $\psi^n$  multiplying the result by  $-(K_{i_1}^2 + K_{i_2}^2 + \dots + K_{i_N}^2)$  and performing an inverse transform back to the spatial domain. In the numerical application, the derivatives are calculated by fast Fourier transform (FFT).

The time derivatives in (2.1) are approximated by second order differencing according to

$$\frac{\partial \psi^n}{\partial t}(i_1, i_2, \dots, i_N) = \frac{\psi^{n+1}(i_1, i_2, \dots, i_N) - \psi^{n-1}(i_1, i_2, \dots, i_N)}{2\Delta t}. \quad (2.2)$$

This derivative is of second order accuracy.

With the above spatial and temporal approximations, a typical step of the solution algorithm runs as follows:

- (a) Given  $\psi^n(i_1, i_2, \dots, i_N)$ , calculate  $\nabla^2 \psi^n$  by an  $N$ -dimensional FFT on  $\psi^n$

followed by a multiplication by  $-(K_{i_1}^2 + \dots + K_{i_N}^2)$  and an inverse  $N$ -dimensional transform.

(b) Calculate  $\hat{V}^n(i_1, \dots, i_N)\psi^n$ . ( $\hat{V}^n$  is a known specified function), and in combination with the result from (a), form  $i\hat{H}\psi^n$ .

(c) Calculate  $\psi^{n+1}$  according to (2.2) by

$$\psi^{n+1} = \psi^{n-1} - 2i \Delta t \hat{H} \psi^n.$$

The steps in (a)–(c) are repeated for the desired number of time steps.

To initialize the solution, the method requires both  $\psi^0$  and  $\psi^1$ , whereas input data normally contains only  $\psi^0$ . There the time integration in the first step to obtain  $\psi^1$  from  $\psi^0$  is done with a second order Runge–Cutta scheme which requires only one starting value.

#### a. *Periodicity and Boundary Conditions*

The discrete Fourier method implies periodic boundary conditions in which  $X_{i_N}$  is connected to  $X_{i_1}$ , where  $N$  is the size of the grid in the  $i$ th coordinate. These boundary conditions are natural for describing spatially periodic problems such as surface scattering, or liquid simulation. For problems where the natural boundary conditions are not periodic, an addition of a large potential at the boundaries stops the interference of the wave across the boundaries. The interference can also be eliminated by expanding the grid size. The price in either case is that a portion of the grid is devoted to the elimination of this interference.

#### b. *Dispersion and Stability*

In addition to the dispersion normally associated with Schrödinger wave equations, the Fourier method introduces additional numerical dispersion. When this dispersion becomes too severe, wavelike solutions to (2.1) no longer exist, and exponentially increasing and decreasing solutions appear causing numerical instability. As a rule it is important to minimize numerical dispersion and to define the conditions in which the dispersion of (2.2) will be close to the true analytic dispersion.

Assume a solution to (2.1) of the form

$$\psi^n = \exp\{i(K_1 X_1 + K_2 X_2 + \dots + K_N X_N - \omega t)\}$$

when the potential  $\hat{V}$  is constant. After a substitution of this equation into (2.1) one gets the dispersion relation

$$\frac{\sin \omega \Delta t}{\Delta t} = \frac{1}{2m} \sum_{i=1}^N K_i^2 + V. \quad (2.3)$$

When the time step  $\Delta t$  is small, this relation approaches the analytical dispersion relation for the Schrödinger equation given by

$$\omega = \frac{1}{2m} \sum_{i=1}^N K_i^2 + V.$$

This result is because the term  $\sin \omega \Delta t$  can then be replaced by  $\omega \Delta t$ .

The stability limit of the method is obtained when the rhs of (2.3) is equal to  $1/\Delta t$ . Since the maximum value of  $K_i$  is  $K_i \max = \pi/\Delta x$ , the stability criterion then reads

$$\left| \Delta t \left( \frac{\pi^2}{2m} \sum_{i=1}^N \frac{1}{\Delta X_i^2} + V \right) \right| < 1. \quad (2.4)$$

Figures 1 and 2 show the dispersion related (2.3) for 1-D propagation for two values of the potential  $\hat{V}$ . These figures show that by keeping the ratio  $\alpha = (\pi^2 \Delta t / 2m) \Delta X^2$  less than 0.2, the numerical dispersion differs little from the exact dispersion.

The above analysis does not cover the case of a time or space variable potential  $\hat{V}$ . However, our experience and the examples which are presented show that by adhering to (2.4) at all points in space and time, the abnormal numerical dispersion can be eliminated. As a rule of thumb for the choice of the time step in practical application of the method, one finds first the stability limit. Then the accurate solution is obtained by using  $\Delta t = 0.2 \Delta t \text{ crit}$  which from Figs. 1 and 2 possess a dispersion which is indistinguishable from the correct dispersion relation.

Examining the spatial and temporal discretization of the method, it is possible to use a higher order time differencing scheme. However, since with the present and second order differencing it was shown that spurious dispersion can virtually be

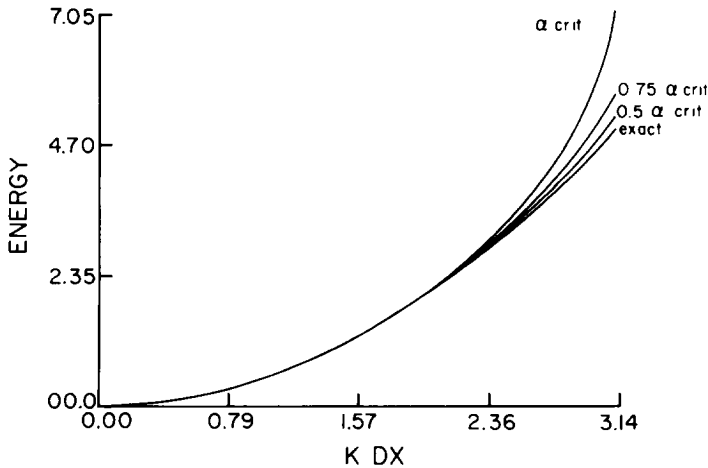


FIG. 1. Dispersion relation for a one-dimensional problem with zero potential.  $\alpha_{\text{crit}} = 1$ , the line with  $\alpha = 0.2\alpha_{\text{crit}}$  is indistinguishable from the exact result.

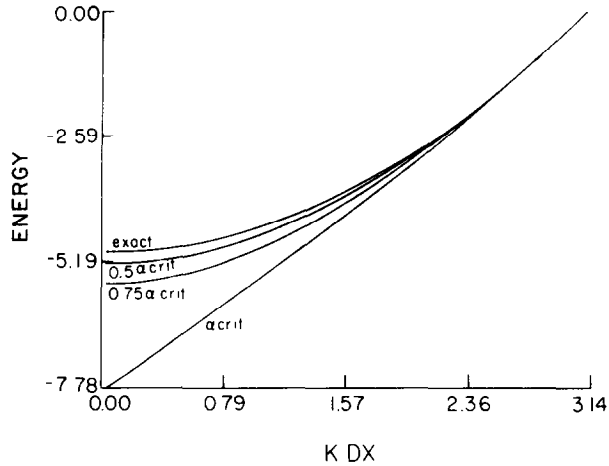


FIG. 2. Dispersion relation for a one-dimensional problem with negative potential.

eliminated, the only justification for a higher order differencing scheme would be a saving in computational time, brought about by an increase in the time step size.

When the dispersion relation of Eq. (2.3) is compared to the dispersion relation obtained by the finite difference method the differences between the methods stick out. Figure 3 gives the dispersion relation for one-dimensional propagation obtained by the explicit second order differencing method of Askar and Cakmak [12]. It shows that at the stability limit  $\Delta t/\Delta x^2 = \frac{1}{2}$  there is a considerable deviation between the true dispersion and the numerical dispersion, and that the deviation increases when the time step  $\Delta t$  is decreased. Apparently in finite difference calculations spurious numerical dispersion will always be present at the short wavelength regardless of the size of the time step. Only at spatial wave numbers smaller than  $\pi/5$

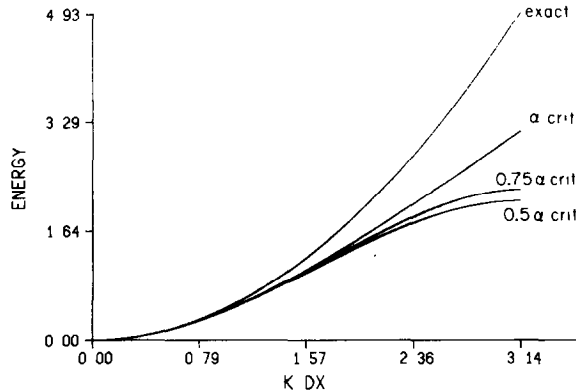


FIG. 3. Dispersion relation for a one-dimensional problem with zero potential for a second order finite difference integrator for zero potential. (The same spatial and temporal grid as Fig. 1).

which corresponds to a wavelength of ten grid points will the numerical dispersion match the exact dispersion relation.

*c. Norm and Energy Conservation and Microscopic Reversibility*

Conservation of norm, energy, and microscopic reversibility, are basic concepts of quantum mechanics. In order for a numerical solution to be of use, it is important that it possesses a discrete analog of these properties.

Considering first the conservation of the norm, Eq. (2.1) is multiplied by  $\psi_n^*$

$$i\psi_n^* \frac{\partial \psi^n}{\partial t} = \psi_n^* \hat{H} \psi^n. \quad (2.5)$$

Next, the conjugate of Eq. (2.1) is taken and multiplied by  $\psi^n$  to get

$$-i\psi^n \frac{\partial \psi_n^*}{\partial t} = \psi^n \hat{H} \psi_n^*. \quad (2.6)$$

After subtracting (2.5) from (2.6) and then summing over all points of the mesh, the result is

$$i \left\langle \psi_n^* \frac{\partial \psi_n^*}{\partial t} \right\rangle + i \left\langle \psi^n \frac{\partial \psi^n}{\partial t} \right\rangle = \langle \psi_n^* \hat{H} \psi_n^* \rangle - \langle \psi^n \hat{H} \psi^n \rangle, \quad (2.7)$$

where the Dirac symbol  $\langle fg \rangle$  is the scalar product  $\sum_{i_1, \dots, i_N} f(i_1, \dots, i_N) g^*(i_1, \dots, i_N)$ . However, the  $\hat{H}$  operator is Hermitian (Appendix A) and the rhs of (2.7) vanishes. Likewise, (2.2) implies

$$\psi_n^* \frac{\partial \psi^n}{\partial t} + \psi^n \frac{\partial \psi_n^*}{\partial t} = (\psi^{n+1} \psi_n^* + \psi_n^{*+1} \psi^n - \psi_n^* \psi^{n-1} - \psi^n \psi_n^{*-1})/2\Delta t$$

and the norm conservation will read

$$\text{Real} \langle \psi^{n+1} \psi^n \rangle = \text{const.} \quad (2.8)$$

Considering next the conservation of energy when the Hamiltonian is time independent, (2.2) is multiplied by  $\partial \psi_n^* / \partial t$  and its conjugate by  $\partial \psi^n / \partial t$ . Summing the result over the mesh gives

$$\left\langle \frac{\partial \psi^n}{\partial t} \hat{H} \psi^n \right\rangle + \left\langle \frac{\partial \psi_n^*}{\partial t} \hat{H} \psi_n^* \right\rangle = 0. \quad (2.9)$$

Using (2.2) the result then becomes

$$\psi^{n+1} \hat{H} \psi_n^* + \psi_n^{*+1} \hat{H} \psi^n = \psi_n^{*-1} \hat{H} \psi^n + \psi^{n-1} \hat{H} \psi_n^*. \quad (2.10)$$

After summing over all grid points and using the Hermitian property of  $\hat{H}$ , the energy conservation law will be obtained

$$\text{Real}\langle\psi^{n+1}\hat{H}\psi^n\rangle = \text{const.} \quad (2.11)$$

This conservation law reduces to the continuous time and space law when the step size is decreased to zero.

In numerical application of the Fourier method, the conservation laws (2.8) and (2.11), were verified to the degree of the precision of the computer.

The microscopic reversibility of the numerical method is a direct consequence of the symmetry of the time derivative approximation. As in the continuous case, when the direction of time is reversed in (2.2), the conjugate discretized equation is obtained.

In addition to the above properties, the commutation relations of the physical space are carried over to the discrete space of the solution (Appendix B). For example,  $[\hat{P}, f(\hat{x})] = -if'(\hat{x})$ , where  $\hat{p} = -i(d/dx)$  is the momentum operator, and  $f$  is a discrete periodic function.

### III. NUMERICAL EXAMPLES

In order to establish confidence in the new method, a few examples are presented. Numerical approximations are compared to exact analytic solutions of non trivial cases.

#### a. *The Potential Step*

The scattering of a wavepacket from a potential step is a text book example which has all the quantum features of expansion of the wavepacket and of interference. As a numerical test, the potential has an infinite derivative and therefore is nontrivial. Fig. 4 presents a few "snapshots" of the absolute value of the wavefunction breaking against the potential step. The main test is the reproduction of the transmittance and reflection coefficients. For a single  $K$  component the reflection coefficient is given by

$$R = \left(\frac{K_1 - K_2}{K_1 + K_2}\right)^2, \quad (3.1)$$

where

$$K_2 = ((E - V) \cdot 2m)^{1/2}.$$

In this study, a Gaussian wavepacket is sent against the potential step. The exact result is obtained by averaging Eq. (3.1) over momentum space. The numerical result is obtained by waiting for the initial wavepacket to separate to the reflected and transmitted part. Figure 5 represents this comparison. As the figure shows, the agreement between the exact and the numerical result is good.

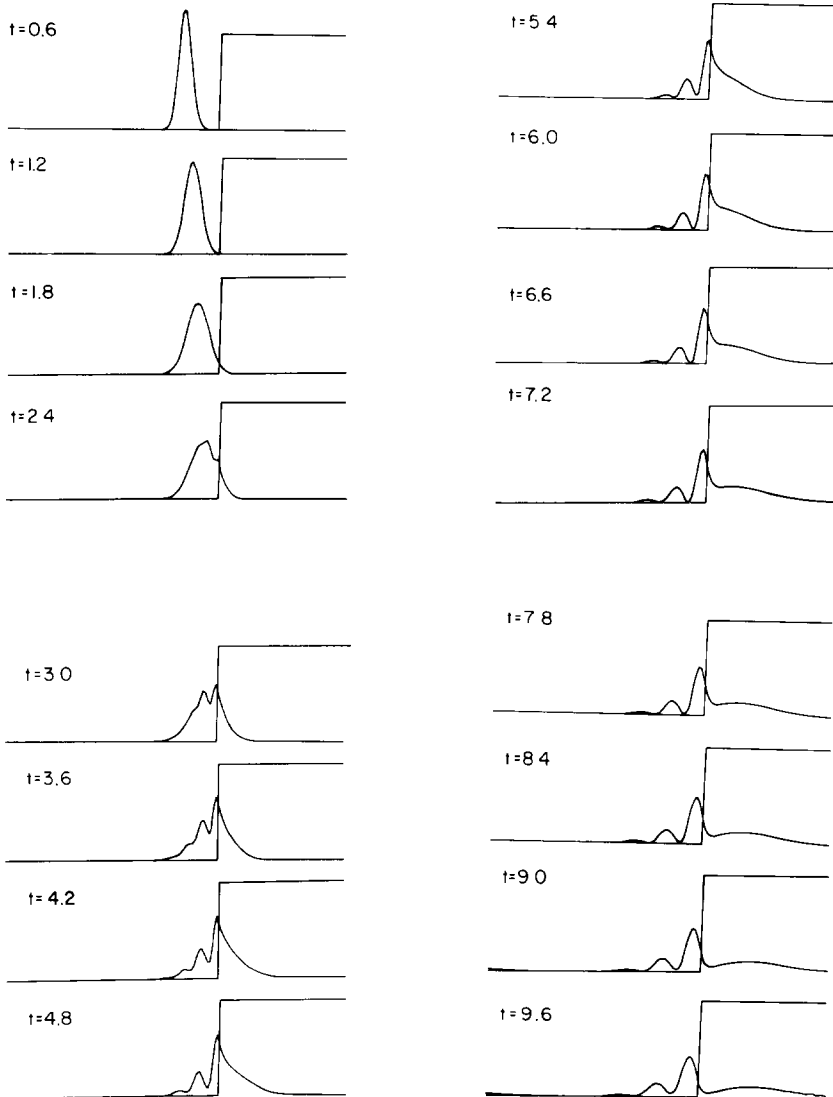


FIG. 4. Snapshots of a wavepacket approaching a potential barrier. The energy of the particle is 1.26 and the barrier height is 1. The grid size is 128 points.

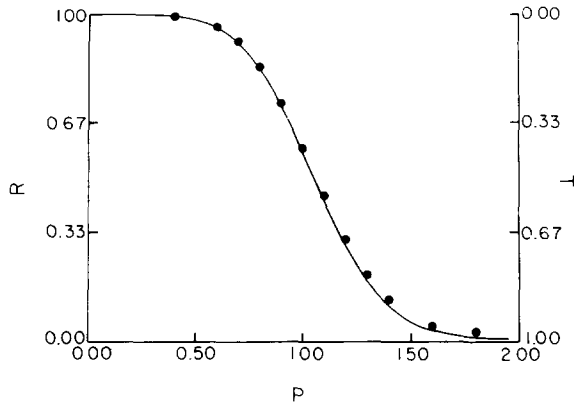


FIG. 5. Reflection and transmittance coefficient as a function of momentum for a Gaussian wavepacket approaching a barrier. The solid line is the exact result, and the points are the numerical approximation calculated with a grid of 256 points.

#### b. The Time Dependent Harmonic Oscillator

The time dependent harmonic oscillator is an important model for considering such phenomena as the multiphoton excitation of molecules. A good numerical solution to this analytically solvable model would mean that the method can be used to deal with more realistic problems such as multiphoton dissociation when the potential is represented by a Morse potential. Work on these lines is in progress [18]. The Hamiltonian of the time dependent harmonic oscillator is

$$\hat{H} = \hat{H}^0 + \hat{q}f(t) \quad \text{with} \quad \hat{H}^0 = \frac{\hat{P}^2}{2m} + \frac{1}{2} K\hat{q}^2. \quad (3.2)$$

$\hat{P} = -i(d/dq)$  is the momentum operator and  $\hat{q}$  is the space operator. A characteristic of the harmonic potential is that it conserves the Gaussian shape of an initial Gaussian wavepacket. The mean value of momentum and position obey the classical equations of motion. This feature was checked numerically for long integration periods and found true.

The energy growth of the time dependent oscillator obeys the relation

$$\Delta \langle \hat{H}^0 \rangle_t = \left| \int_0^t e^{i\omega t} f(t) dt \right|^2. \quad (3.3)$$

When considering resonant excitation, where  $f(t) = \sin \omega t$ , the average energy increases proportionally to  $t^2$  and has a modulation with the frequency  $2\omega$ . Figure 6 presents the outcome of the numerical calculation with a grid of 128 points. The dashed line is the exact average energy; the numerical result follows this line with the expected modulation of  $2\omega$ .

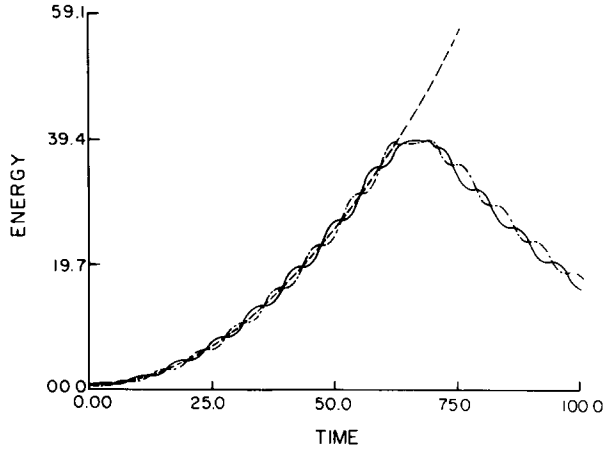


FIG. 6. Energy as a function of time for a resonant driven harmonic oscillator. The solid line is the average analytic energy growth;  $\langle \hat{H}^0 \rangle$  (---),  $\langle \hat{H}^0 + \hat{V}(t) \rangle$  (- · - · - ·).

An interesting feature is revealed when the numerical result stops following the exact solution. This happens when the energy obtained exceeds the highest possible momentum (wave number) value of the grid. Following the solution, the energy starts to decrease and a beginning of a periodic solution emerges. This periodic solution is a consequence of finite Hilbert space used to approximate the harmonic oscillator. In a finite Hilbert space, all operators are bound and a periodic perturbation will always lead to a periodic solution [8]. Increasing the grid will raise the energy in which the exact solution deviates from the numerical one. Using this scheme for considering realistic potentials, the dissociation energy provides a natural limit for which the grid size can be set.

### c. The Two-Dimensional Kepler Problem

A multidimensional application of the Fourier method to the two-dimensional Kepler problem is an important example of the approach of this paper, and it has realistic significance as a model for thin films of Cesium. In the application, the periodic boundary represents a physical reality. In this example the potential has a singular point and is long range. The analytic results are obtained by transforming to separable coordinates  $R$  and  $\theta$ . However, since the test is performed in  $X$  and  $Y$  coordinates (where the problem is not separable), it is numerically difficult.

By solving the analytic problem, one obtains the energy spectrum

$$E_{nm} = \frac{-2Z}{(2n + 2m + 1)^2}. \quad (3.4)$$

For the eigenfunctions one obtains

$$\psi_{nn} = N_{nm} e^{-K_{nm}r} r^m L_n^{2|m|} (2K_{nm}r) e^{im\phi}, \quad (3.5)$$

TABLE I  
Spectrum of the First Ten States of the Two-Dimensional Kepler Problem

$m$	$n$	0	1	2	3
	0		-2.0000 -1.9458	-0.22222 -0.20795	-0.08000 -0.07325
1		-0.22222 -0.22213	-0.08000 -0.07999	-0.040816 -0.040815	
2		-0.08000 -0.08002	-0.040816 -0.040816		
3		-0.040816 -0.040745			

*Note.* The upper values are the exact ones and the lower are the numeric approximation.

where

$$K_{nm} = \frac{Z}{2n + 2m + 1}$$

and  $L_n^m(x)$  are the associated Laguerre polynomials. The first check of the discrete Hamiltonian, the energy spectrum is calculated for the first ten eigenfunctions by inserting Eq. (3.5) into Eq. (2.11). Table I represents a comparison between the exact and numerical calculations. By examining Table I, one can see that there is a good

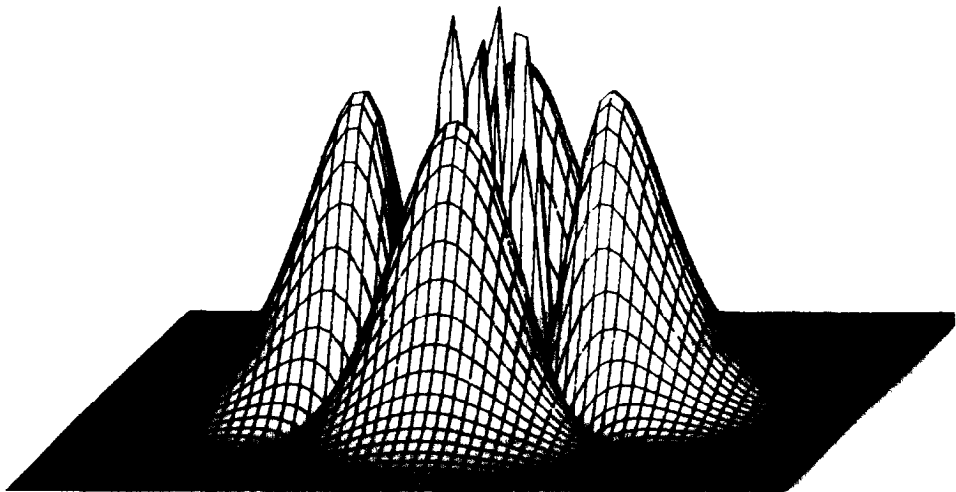
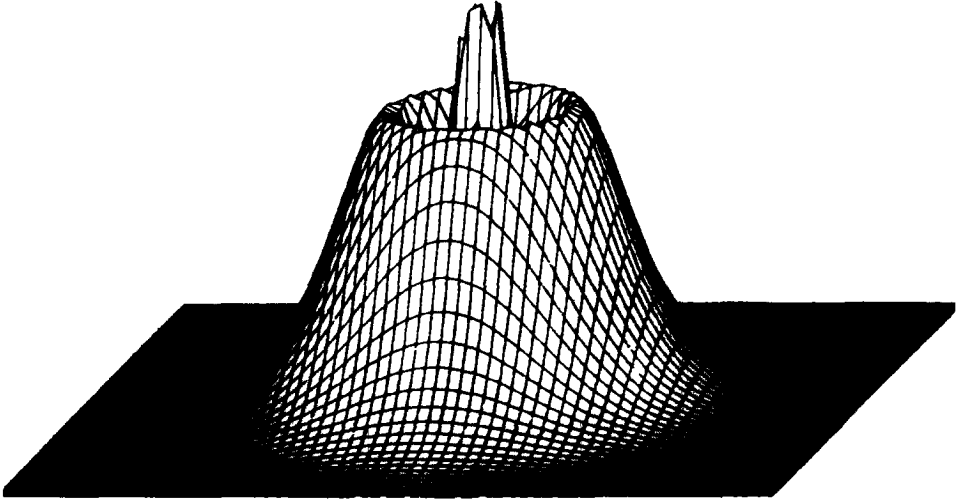
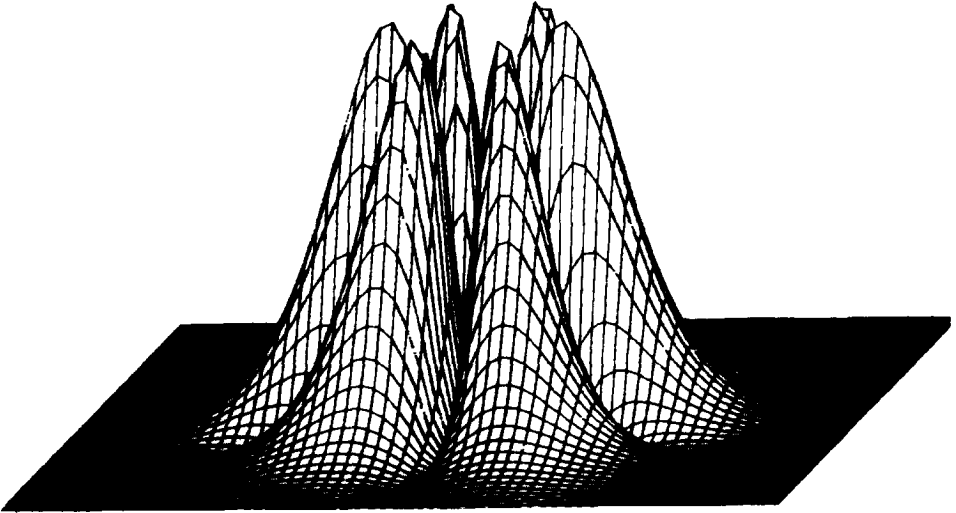
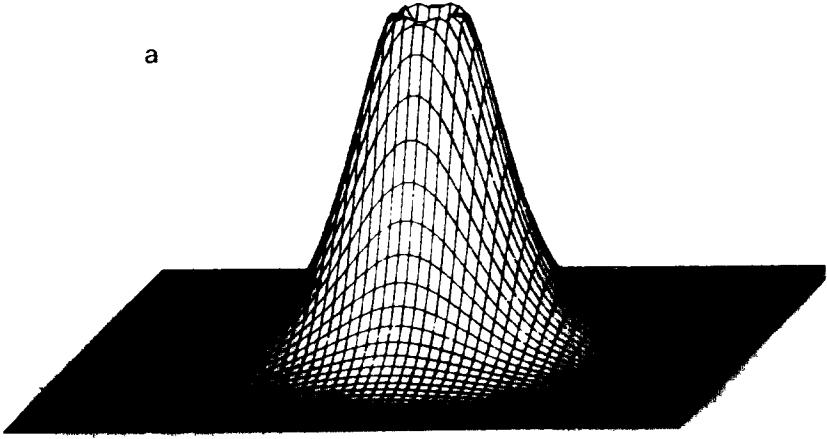


FIG. 7a. Excited stationary states of the two-dimensional Kepler problem. The state  $(\psi_{21} + \psi_{2-1})(1/\sqrt{2})$ .

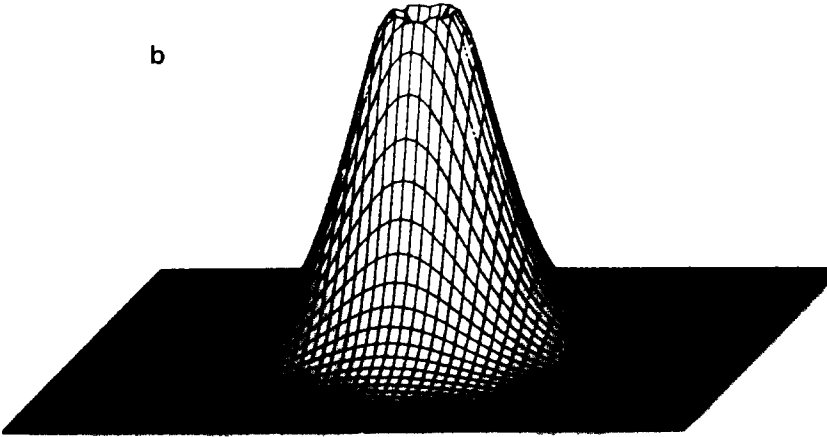
FIG. 7b. The excited state  $\psi_{30}$ .FIG. 7c. The excited state  $(\psi_{03} + \psi_{0-3})(1/\sqrt{2})$ .

numerical approximation for all states with nonzero angular momentum. This is because these states are zero at the origin, and therefore are not affected by the full extent of the singularity in the potential. Since the  $m = 0$  states are less accurate, improvement of accuracy means increase in the grid size. Another check of the numerical approximation is to use the analytic wave functions as initial states which are integrated in time. If the analytic wave functions are stationary in the discrete

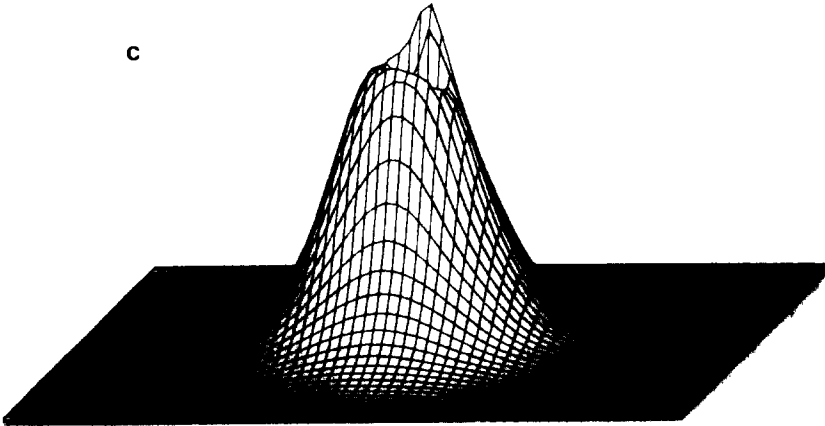
a



b



c



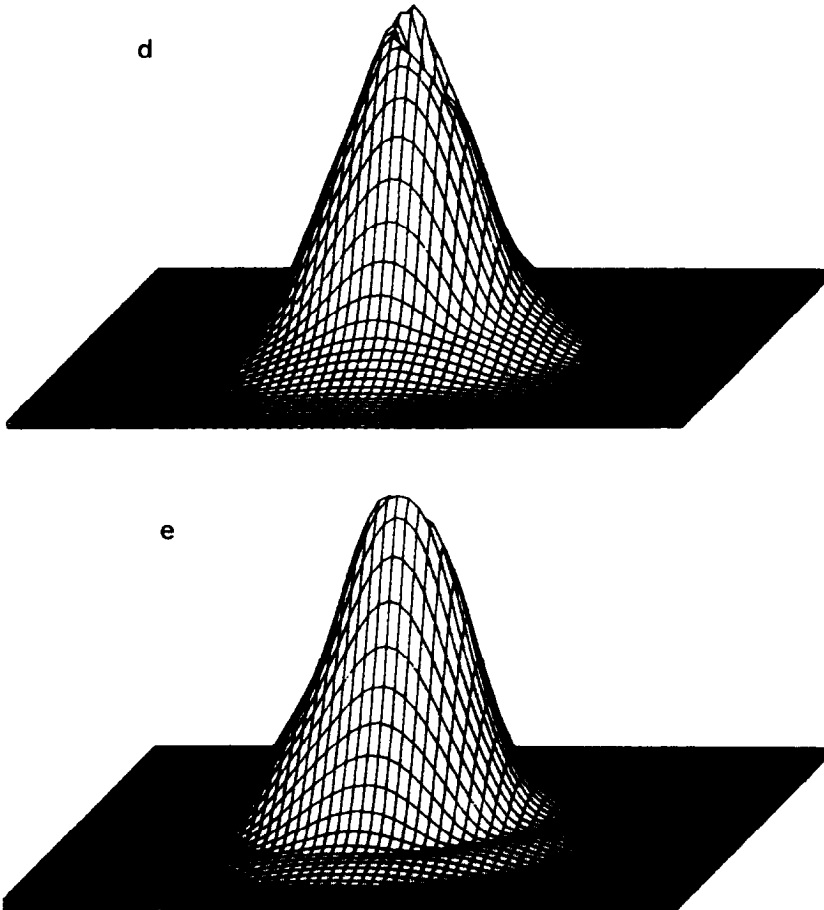


FIG. 8. Snapshots of an initial stationary state perturbed by a periodic time dependent potential. The initial state is  $\psi_{01}$ . The frequency of perturbation is  $\omega = 1.7777$  which is resonant to the  $\psi_{01} \rightarrow \psi_{11}$  transition and to a transition to unbound states. Snapshots are at  $\Delta t = 1.6$  units apart. The energy changes in time: (a)  $E = -0.222$ , (b)  $E = -0.189$ , (c)  $E = -0.123$ , (d)  $E = -0.385$ , (e)  $E = +0.112$ .

world, the overlap  $|\langle \psi^0, \psi^n \rangle|^2$  should be unity. For a grid of  $64 \times 64$  a deviation of 4% was found for state  $\psi_{10}$  after 4 a.t.u. (atomic time units). For a grid of  $128 \times 128$ , deviations for the states  $\psi_{10}$ ,  $\psi_{10}$ ,  $\psi_{21}$  and  $\psi_{03}$  were less than .1% for similar periods of time. This means that the solution has converged.

A typical time step on a  $128 \times 128$  grid took 20 sec on a VAX 750 with a floating point unit. A typical run took 500 steps. Fig. 7 represents a few of the excited stationary states of the Kepler problem. Figure 8 represents a time dependent solution where the initial state is  $\psi_{01}$ , perturbed by a periodic time dependent linear potential. This perturbation simulates an interaction with the electromagnetic field. As Fig. 7 shows, the otherwise stationary state is scattered.

## IV. DISCUSSION

One of the most important issues of quantum mechanics [20] is the relation between observables and the operators that represent them, and it has been stated that there is a one-to-one correspondence between the observables and the operators. Moreover, the operators that represent observables are Hermitian because observables are real and Hermitian operators have real eigenvalues. In constructing a numerical approximation to the time dependent Schrödinger equation these ideas were behind the logic that led to the use of the Fourier method. The discrete space on which the approximation is based is a Hilbert space. Operators which correspond to observables which are Hermitian in the physical Hilbert space, are mapped into Hermitian operators in the discrete space. (As Askar showed, this is not true in the finite difference method.) Moreover, commutation relations which are at the heart of quantum dynamics, are preserved in the mapping scheme from the physical to the discrete space. On this basis, the discrete Hilbert space is a physical world to itself which possesses all the qualities of quantum mechanics. This Hilbert space converges to the true physical world when the grid size is large enough.

Another important advantage of the Fourier method from the numerical point of view is that numerical dispersion can be eliminated at all frequencies. Therefore the calculations are valid for all wavelengths that are represented on the spatial grid. A good demonstration of this feature is the example of the time dependent harmonic oscillator where energy is pumped in and the numerical solution follows the analytic solution almost to the maximum frequency represented on the grid. This is in contrast with the finite difference method where spurious numerical dispersion is always present. The dispersion curve for finite difference shows that artificial numerical dispersion is small only for wavelengths larger than ten grid points. This means that for comparable accuracy, the Fourier method requires a factor of five less grid points for each spatial dimension. This fact becomes extremely important in multidimensional calculations (3-D). Admittedly, because the Fourier method uses a nonlocal function expansion the number of operations per grid point is higher than with the finite difference method. However, utilization of the fast Fourier transform (FFT) algorithm immensely improves numerical efficiency. Aside from its accuracy the Fourier method is completely vectorizable and therefore will work well on vector computers and array processors. The reduction in the number of grid points is extremely important for multidimensional problems.

Comparing the Fourier method to standard functional expansion methods, it appears that the two approaches are complementary. When there is a good knowledge of the problem and conditions of symmetry can be used, expansion methods are efficient. This is because the number of expansion functions can be kept small. For more general problems, where there is no natural expansion, a direct solution method is preferable. An interesting possibility would be the use of hybrid methods which would use function expansion for part of the spatial dimensions, and a Fourier method for the remaining dimensions.

Altogether it can be concluded that the Fourier method has a promising potential

as a routine tool in the study of molecular dynamics. One of the main reasons is that the approximation is controllable so that accurate and stable results are obtainable. Another reason is that the method has numerical efficiency especially with the new generation of vector computers.

#### APPENDIX A: HERMITIAN PROPERTIES OF THE FOURIER METHOD

In this appendix it is proven that in the discrete Hilbert space, the Hamiltonian is Hermitian. For any two functions  $u$  and  $v$  this property is written

$$\langle u\hat{H}v \rangle = \langle v\hat{H}u \rangle, \quad \text{where } \hat{H} = -\frac{1}{2m}\hat{\nabla}^2 + \hat{V}^n.$$

Concerning the potential operator  $\hat{V}^n$  it is a multiplication operator, and therefore obviously Hermitian. It remains to be shown that any of the terms  $\partial^2/\partial x_i^2$  in the definition of  $\hat{\nabla}^2$ , is Hermitian. The first step is to prove two lemmas.

LEMMA 1. *With the Fourier method*

$$\frac{d}{dx}(fg) = \frac{df}{dx}g + f\frac{dg}{dx} \quad (\text{A.1})$$

for any functions  $f, g$ .

*Proof.* Since  $\widetilde{(f, g)} = \tilde{f} * \tilde{g}$ , where  $*$  defines a convolution and  $\tilde{\phantom{x}}$  denotes a spatial Fourier transform, one obtains

$$\begin{aligned} \frac{d}{dx}\widetilde{fg} &= iK_x \sum_{K'_x} \tilde{f}(K'_x) \tilde{g}(K_x - K'_x) \\ &= \sum_{K'_x} \tilde{f}(K'_x) i(K_x - K'_x) \tilde{g}(K_x - K'_x) + iK'_x \tilde{f}(K'_x) \tilde{g}(K_x - K'_x) \\ &= \sum_{K'_x} \tilde{f}(K'_x) \frac{d\tilde{g}}{dx}(K_x - K'_x) + \frac{d\tilde{f}}{dx}(K'_x) \tilde{g}(K_x - K'_x). \end{aligned} \quad (\text{A.2})$$

The inverse transform of (A.2) proves (A.1).

LEMMA 2.

$$\nabla \frac{df}{dx} = 0 \quad (\text{A.3})$$

for any function  $f$ .

*Proof.* By the property of FFT,

$$\nabla \frac{df}{dx} = \frac{df(0)}{dx} \quad (\text{A.4})$$

but  $d\tilde{f}/dx = iK\tilde{f}$ ... and therefore (A.4) gives zero. Returning to the term  $u(\partial^2 v/\partial x_i^2)$  by applying Lemma 1 one obtains

$$\begin{aligned} u \frac{\partial^2 v}{\partial x_i^2} &= \frac{\partial}{\partial x_i^2} \left( u \frac{\partial v}{\partial x_i} \right) - \frac{\partial u}{\partial x_i} \frac{\partial v}{\partial x_i} \\ &= \frac{\partial}{\partial x_i} u \frac{\partial v}{\partial x_i} - \frac{\partial}{\partial x_i} v \frac{\partial u}{\partial x_i} + \frac{\partial^2 u}{\partial x_i^2} v \end{aligned} \quad (\text{A.5})$$

upon forming the inner product  $\langle u(\partial^2 v/\partial x_i^2) \rangle$  as in (A.5). The first three terms on the rhs give zero. In view of Lemma 2 the term  $\langle \partial^2 u/\partial x_i^2, v \rangle$  remains, thus completing the proof of the Hermitian property of  $\hat{H}$ .

## APPENDIX B: COMMUTATION PROPERTIES OF THE FOURIER METHOD

The discrete numerical approximation obeys the same commutation relations for functions of momentum and position as the original physical space. For any operators  $\hat{A}, \hat{B}$  the commutation relation is defined as

$$[\hat{A}\hat{B}] = \hat{A}\hat{B} - \hat{B}\hat{A}. \quad (\text{B.1})$$

Consider the relation between the momentum operator  $\hat{p} = -i(\partial/\partial x)$  and a function of the position operator  $f(\hat{x})$  in one spatial dimension. With the product differentiation rule obtained in Appendix A, one gets

$$[\hat{p}, f(\hat{x})]g = -i \frac{\partial}{\partial x} f(\hat{x})g - f(\hat{x})i \frac{\partial g}{\partial x} = -if'(\hat{x})g \quad (\text{B.2})$$

for any discrete function  $f$ . Therefore

$$[\hat{p}, f(\hat{x})] = -if'(\hat{x}). \quad (\text{B.3})$$

In (B.2) and (B.3) it is understood that the derivatives are calculated by the Fourier method. When the operator  $f(\hat{x})$  is band limited and bounded in the grid. Derivatives by the Fourier approximation are exact [21] in such cases and therefore the commutation relation (B.3) is equal to the commutation relation of the physical space.

## ACKNOWLEDGMENTS

This work was supported by the Bat-Sheva Foundation. The Fritz Haber Research Center is supported by the Minerva Gesellschaft für die Forschung, *GmbH*, Munich, FRG. The authors wish to thank M. Cohen for help on the analytic solution of the two-dimensional Kepler problem and O. Viner for computational help and J. Kadmon for editing.

## REFERENCES

1. R. D. LEVINE, "Quantum Mechanics of Molecular Rate Processes," (Clarendon), Oxford Univ. Press London, 1969.
2. W. N. SAMS AND D. J. KOURI, *J. Chem. Phys.* **64** (1976), 1621; 1640; 1941.
3. R. GORDON, *J. Chem. Phys.* **51** (1969), 141; *Methods Comput. Phys.* **10** (1971), 81.
4. E. J. MCGUIRE, *Phys. Rev.* **51** (1970) 101; **20** (1968), 175.
5. D. SECREST AND B. R. JOHNSON, *J. Chem. Phys.* **48** (1968), 4682.
6. J. C. LIGHT AND R. B. WALKER, *J. Chem. Phys.* **65** (1976), 4272.
7. A. ASKAR, *J. Chem. Phys.* **74** (1981), 6133.
8. S. C. LEASURE, K. F. MILFELD, AND R. WYATT, *J. Chem. Phys.* **74** (1981), 6197; S. C. LEASURE AND R. WYATT, *Opt. Eng.* **19** (1980), 46.
9. S. Y. LEE AND E. J. HELLER, *J. Chem. Phys.* **76** (1982), 3035.
10. J. FRENKEL, "Wave Mechanics," Oxford Univ. Press (Clarendon), London, 1934; A. D. MCLACHLAN, *Mol. Phys.* **8** (1964), 39.
11. E. A. MCCULLOUGH AND R. E. WYATT, *J. Chem. Phys.* **51** (1969), 1253; **54** (1971), 3578; **54** (1971) 3592; K. C. KULANDER, *J. Chem. Phys.* **69** (1978), 5064.
12. A. ASKAR AND A. S. CAKMAK, *J. Chem. Phys.* **68** (1978), 2794.
13. R. B. WALKER AND R. P. PRESTON, *J. Chem. Phys.* **67** (1977), 2017.
14. B. FORENBERG, *SIAM J. Numer. Anal.* **12** (1975), 509; B. FORENBERG AND G. B. WILLIAM, *Philos. Tran. Roy. Soc. London Ser. A* **289** (1978), 373.
15. S. A. ORSZAG, *J. Comput. Phys.* **37** (1980), 93.
16. H. O. KREISS AND J. OLIGER, *Tellus* **24** (1972), 199.
17. J. GAZDAG, *Geophysics* **46** (1981), 854.
18. D. KOSLOFF AND E. BAYSAL, 1982, to appear.
19. R. KOSLOFF AND D. KOSLOFF, *J. Chem. Phys.* (1983), in press.
20. J. VON NEUMANN, "Mathematical Foundations of Quantum Mechanics," Princeton Univ. Press, Princeton, N.J., 1955.
21. R. N. BRACEWELL, "The Fourier Transfer and Its Application," 2nd ed. McGraw-Hill, New York, 1978.